



BIFURCATION AND OVEREXPLOITATION IN ROSENZWEIG–MACARTHUR MODEL

XIAOQING LIN AND YANCONG XU*

Department of Mathematics, Hangzhou Normal University
Zhejiang 311121, China

DAOZHOU GAO

Department of Mathematics, Shanghai Normal University
Shanghai 200234, China

GUIHONG FAN

Department of Mathematics, Columbus State University
Columbus, GA 31907, USA

(Communicated by Gail Wolkowicz)

ABSTRACT. In this paper, we propose a Rosenzweig–MacArthur predator-prey model with strong Allee effect and trigonometric functional response. The local and global stability of equilibria is studied, and the existence of bifurcation is determined in terms of the carrying capacity of the prey, the death rate of the predator and the Allee effect. An analytic expression is employed to determine the criticality and codimension of Hopf bifurcation. The existence of supercritical Hopf bifurcation and the non-existence of Bogdanov–Takens bifurcation at the positive equilibrium are proved. A point-to-point heteroclinic cycle is also found. Biologically speaking, such a heteroclinic cycle always indicates the collapse of the system after the invasion of the predator, i.e., overexploitation occurs. It is worth pointing out that heteroclinic relaxation cycles are driven by either the strong Allee effect or the high per capita death rate. In addition, numerical simulations are given to demonstrate the theoretical results.

1. Introduction. Since predator and prey populations can grow, disappear or remain unchanged over time, depending on their birth rates, mortality, immigration and emigration, it is necessary to consider mathematical models which describe the environment. By using the dynamical system approach [5, 6], it has been shown that different predator functional responses in the Rosenzweig–MacArthur model exhibit different effects on the dynamics of the model [22, 29, 11, 25]. Sugie and Saito [29] studied the Rosenzweig–MacArthur predator-prey model with a Holling type II functional response and derived necessary and sufficient conditions for the

2020 *Mathematics Subject Classification.* Primary: 58F15, 58F17; Secondary: 53C35.

Key words and phrases. Rosenzweig–MacArthur model, strong Allee effect, trigonometric functional response, overexploitation.

The second author is supported by the National NSF of China (No. 11671114) and NSF of Zhejiang Province(LY20A010002); The third author is supported by NSF of Shanghai (20ZR1440600, 20JC1413800).

* Corresponding author: Yancong Xu.

uniqueness of limit cycles. The most consistently useful mathematical representation of the real data was formed to be the trigonometric tangent function, which precisely describes the relationship between photosynthesis and light for phytoplankton and was used by Jassby and Platt [16]. Fussmann and Blasius [11] proposed a Rosenzweig–MacArthur model to describe the community dynamics with three different functional responses including Holling type II functional response ($\Phi(N) = \frac{aN}{1+bN}$), Ivlev functional response ($\Phi(N) = a(1 - e^{-bN})$), and trigonometric functional response ($\Phi(N) = a \tanh(bN)$). It has been shown that the response function with the trigonometric form has the lowest potential to collapse Rosenzweig–MacArthur model dynamics.

Seo and Wolkowicz [25] considered the following Rosenzweig–MacArthur model:

$$\begin{aligned} \frac{dN}{dt} &= rN \left(1 - \frac{N}{K}\right) - \Phi(N)P, \\ \frac{dP}{dt} &= (\Phi(N) - m)P, \end{aligned} \tag{1}$$

where $\Phi(N) = \alpha \tanh(bN)$ is the trigonometric functional response, the variables N and P represent the numbers of prey and predators, respectively. r is the intrinsic growth rate of the prey, K is the carrying capacity, m is the per capita mortality rate of the predator. All parameters r, m, α, b and K are assumed to be positive. The tipping point of subcritical Hopf bifurcation and supercritical Hopf bifurcation, i.e., a saddle-node bifurcation point of limit cycles, induced by the trigonometric functional response was investigated numerically, while for Holling type II functional response $\Phi(N) = \frac{aN}{1+bN}$ or Ivlev functional response $\Phi(N) = a(1 - e^{-bN})$, system (1) only can give rise to supercritical Hopf bifurcation, i.e., there is a stable limit cycle emanating from it.

The concept of Allee effect was initially proposed by American ecologist Warder Allee [2]. It describes a positive relationship between any component of individual fitness and either number or density of conspecifics in Stephen et al. [28]. Clustering is good for population growth and survival, but too sparse or too crowded will have negative effects. In nature, many species have Allee effects, such as animals [3, 33], plants [9, 27], plants and animals [19]. There are two types of Allee effects: weak Allee effect [4, 24] and strong Allee effect [1, 10, 13, 18, 21, 31, 32]. Berec et al. [3] demonstrated that the speed of mate search determines the intensity of the Allee effect, and found that it is mainly male prey that evolves towards the maximum mate search rate, thus generating the weakest Allee effect in mate search or evolutionary bistability. Petrovskii et al. [20] investigated that patchy invasion seems possible in a fully deterministic predator-prey model due to the Allee effect. Therefore, we consider the role of the Allee effect in the Rosenzweig–MacArthur model to study possible dynamics.

In this paper, we consider a Rosenzweig–MacArthur model with the strong Allee effect and the trigonometric functional response as follows:

$$\begin{aligned} \frac{dN}{dt} &= rN \left(1 - \frac{N}{K}\right) (N - v) - \alpha \tanh(bN)P \doteq q(N) - \Phi(N)P, \\ \frac{dP}{dt} &= (\alpha \tanh(bN) - m)P \doteq (\Phi(N) - m)P, \end{aligned} \tag{2}$$

with initial conditions $N(0) > 0$ and $P(0) > 0$. Here the parameter $v > 0$ is a threshold population level which represents the Allee effect. According to the

nature of the hyperbolic tangent function, the trigonometric functional response $\Phi(N) = \alpha \tanh(bN)$ is monotonically increasing, and satisfies $\Phi(0) = 0$ and $\Phi'(N) = \alpha b \operatorname{sech}^2(bN) > 0$ for all $N > 0$. The growth function $q(N) = rN \left(1 - \frac{N}{K}\right) (N-v)$ has an enhanced growth rate as the population increases above the threshold population value. If $q(0) = 0$ and $q'(0) \geq 0$ as $v \leq 0$, then $q(N)$ represents a proliferation exhibiting a weak Allee effect, whereas if $q(0) = 0$ and $q'(0) < 0$ as $v > 0$, then $q(N)$ represents a proliferation exhibiting a strong Allee effect ($v > 0$). With weak Allee effect the population growth rate at low population densities is still positive, though not at its maximum value. But in the strong Allee effect, below the threshold v , the population growth rate is negative and the population becomes negative.

The rest of this paper is organized as follows. In section 2, we rescale model (2) to obtain the number of equilibria and the basic reproduction number of the dimensionless system. In section 3, using a linearized method, we conduct the local stability analysis of four equilibria. In section 4, we derive the codimension of Hopf bifurcation, the existence of heteroclinic cycle and the non-existence of Bogdanov-Takens bifurcation for the positive equilibrium. Note that a heteroclinic orbit always indicates that overexploitation occurs [1, 15, 32], i.e., the predator invasion can fail and lead to system collapse. In section 5, numerical simulations are presented to illustrate the main results. Further, the existence of heteroclinic relaxation oscillation cycles is also found numerically when the per capita mortality rate of the predator or the strong Allee effect is large enough. Finally, some conclusions and discussions are also given.

2. Equilibria and basic reproduction number. To simplify the analysis in the following sections, introducing the change of variables

$$P = \frac{X}{b}, \quad N = \frac{Y}{b}, \quad \tau = \alpha t, \quad (3)$$

reduces the system (2) to

$$\begin{aligned} \frac{dX}{d\tau} &= X(\tanh(Y) - A), \\ \frac{dY}{d\tau} &= BY(D - Y)(Y - C) - X \tanh(Y), \end{aligned} \quad (4)$$

where

$$A = \frac{m}{\alpha}, \quad B = \frac{r}{\alpha b^2 K}, \quad C = vb, \quad D = Kb. \quad (5)$$

Similarly, if we take $A = \frac{m}{\alpha}$, $\bar{B} = \frac{r}{\alpha b K}$, $D = Kb$, then the dimensionless form of model (1) becomes

$$\begin{aligned} \frac{dX}{d\tau} &= X(\tanh(Y) - A), \\ \frac{dY}{d\tau} &= \bar{B}Y(D - Y) - X \tanh(Y). \end{aligned} \quad (6)$$

Setting the right-hand side of system (4) equals zero gives the following equilibria of system (4): one trivial equilibrium $E_0(0, 0)$, two boundary equilibria $E_1(0, C)$ and $E_2(0, D)$, and one positive equilibrium $E_3(X_3, Y_3)$, where $X_3 = \frac{B}{A}Y_3(D - Y_3)(Y_3 - C)$ and $Y_3 = \tanh^{-1}(A)$. Since $K > v > 0$, then we have $D > C > 0$. Thus, the positive equilibrium E_3 exists for $0 < C < Y_3 < D$.

Note that model (6) has three equilibria: $\bar{E}_0(0, 0)$, $\bar{E}_2(0, D)$ and $\bar{E}_3(\bar{X}_3, \bar{Y}_3)$, where $\bar{X}_3 = \frac{B}{A}\bar{Y}_3(D - \bar{Y}_3)$, and $\bar{Y}_3 = \tanh^{-1}(A)$ satisfying $0 < \bar{Y}_3 < D$. Next, the

basic reproduction number is obtained by using the next generation matrix method developed by van den Driessche and Watmough [30]. System (4) can be rewritten as

$$\frac{dZ(\tau)}{d\tau} = f(Z) - v(Z),$$

where

$$Z = \begin{pmatrix} X \\ Y \end{pmatrix}, f(Z) = \begin{pmatrix} X \tanh(Y) \\ 0 \end{pmatrix},$$

$$v(Z) = \begin{pmatrix} AX \\ -BY(D - Y)(Y - C) + X \tanh(Y) \end{pmatrix}.$$

The matrices $\mathbb{F}(Z)$ and $\mathbb{V}(Z)$ are defined as

$$\mathbb{F}(Z) = \begin{pmatrix} \tanh(Y) & X \operatorname{sech}^2(Y) \\ 0 & 0 \end{pmatrix}, \mathbb{V}(Z) = \begin{pmatrix} A & 0 \\ \tanh(Y) & \eta(X, Y) \end{pmatrix},$$

and

$$\mathbb{V}^{-1}(Z) = \begin{pmatrix} \frac{1}{A} & 0 \\ -\frac{\tanh(Y)}{A\eta(X, Y)} & \frac{1}{A\eta(X, Y)} \end{pmatrix},$$

where $\eta(X, Y) = -B(D - Y)(Y - C) + BY(Y - C) - BY(D - Y) + X \operatorname{sech}^2(Y)$. Hence, the basic reproduction number of system (4) can be defined as the spectral radius of the next generation matrix $\mathbb{F}\mathbb{V}^{-1}$, given by

$$R_0 = \rho(\mathbb{F}\mathbb{V}^{-1}) = \frac{\tanh(C)}{A} \doteq \frac{\tanh(C)}{\tanh(Y_3)}. \quad (7)$$

3. Stability of equilibria. The Jacobian matrix of system (4) at any equilibrium E is

$$J(E) = \begin{pmatrix} \tanh(Y) - A & X \operatorname{sech}^2(Y) \\ -\tanh(Y) & -\eta(X, Y) \end{pmatrix}.$$

Since the X -coordinates of equilibria E_0, E_1, E_2 equal 0, the eigenvalues of the Jacobian matrices at E_0, E_1 and E_2 are

$$\lambda_1 = \tanh(Y) - A \quad \text{and} \quad \lambda_2 = B(D - Y)(Y - C) - BY(Y - C) + BY(D - Y).$$

(1) The Jacobian matrix $J(E)$ evaluated at $E_0 = (0, 0)$ has two characteristic roots

$$\lambda_{1E_0} = -A < 0 \quad \text{and} \quad \lambda_{2E_0} = -BDC < 0.$$

Hence, E_0 is always a stable node.

(2) The Jacobian matrix $J(E)$ evaluated at $E_1 = (0, C)$ has two characteristic roots with

$$\lambda_{1E_1} = \tanh(C) - A > 0 \quad (R_0 > 1) \quad \text{and} \quad \lambda_{2E_1} = BC(D - C) > 0.$$

Therefore, E_1 is an unstable node. Or if

$$\lambda_{1E_1} = \tanh(C) - A < 0 \quad (R_0 < 1),$$

then E_1 is a saddle point.

(3) The Jacobian matrix $J(E)$ evaluated at $E_2 = (0, D)$ has two characteristic roots with

$$\lambda_{1E_2} = \tanh(D) - A < 0 \quad \text{for} \quad \tanh(D) < A, \quad \text{and} \quad \lambda_{2E_2} = -BD(D - C) < 0.$$

This claims that E_2 is a stable node. If

$\lambda_{1_{E_2}} = \tanh(D) - A > 0$ for $\tanh(D) > A$, and $\lambda_{2_{E_2}} = -BD(D - C) < 0$, then E_2 is a saddle point. It is easy to see that $\tanh(D) - A > \tanh(C) - A > 0$, i.e., E_2 is always a saddle when E_1 is an unstable node. Furthermore, the characteristic equation of system (4) at the positive equilibrium E_3 is

$$\lambda^2 - \text{tr}(J(E_3))\lambda + \det(J(E_3)) = 0, \quad (8)$$

where

$$\begin{aligned} \text{tr}(J(E_3)) &= \frac{B}{\tanh(Y_3)} \text{tr}^*(J(E_3)), \\ \det(J(E_3)) &= \frac{BY_3}{\cosh^2(Y_3)} (D - Y_3)(Y_3 - C), \end{aligned} \quad (9)$$

and $\text{tr}^*(J(E_3)) = -Y_3(D - Y_3)(Y_3 - C)(1 - \tanh^2(Y_3)) - [3Y_3^2 - 2(C + D)Y_3 + CD] \tanh(Y_3)$. It is easy to see that $\det(J(E_3)) > 0$ when E_3 exists. The stability of E_3 is thus determined by the sign of $\text{tr}^*(J(E_3))$: E_3 is stable when $\text{tr}^*(J(E_3)) < 0$, and unstable if $\text{tr}^*(J(E_3)) > 0$. Note that E_3 becomes a Hopf bifurcation point as $\text{tr}^*(J(E_3)) = 0$.

Next, model (4) will be analyzed in a biologically feasible region

$$\mathbb{R}_+^2 = \{(X, Y) \in \mathbb{R}^2 : X \geq 0 \text{ and } Y \geq 0\}.$$

Proposition 1. *All solutions of system (4) converge to $E_0(0, 0)$ if $R_0 > 1$.*

Proof. Consider the following Lyapunov function

$$V(X, Y) = AX + \tanh(C)Y, \quad (10)$$

which satisfies $V(E_0) = 0$. Differentiating V with respect to τ along the trajectory of system (4) yields

$$\begin{aligned} \left. \frac{dV}{d\tau} \right|_{(4)} &= AX \tanh(Y) - A^2 + \tanh(C)BY(D - Y)(Y - C) - \tanh(C)X \tanh(Y) \\ &= (A - \tanh(C))X \tanh(Y) - A^2. \end{aligned}$$

Since we only consider the region in $\{(X, Y) \in \mathbb{R}^2 : X \geq 0, 0 \leq Y \leq D\}$, it is easy to see that $\left. \frac{dV}{d\tau} \right|_{(4)} < 0$ as $A - \tanh(C) < 0$, i.e., $R_0 > 1$. Hence, all solutions of system (4) converge to $E_0(0, 0)$ if $R_0 > 1$. \square

4. Bifurcation analysis.

4.1. Hopf bifurcation. Hopf bifurcation may occur in system (4) when the positive equilibrium E_3 exists. By using (9), we know that $\det(J(E_3)) > 0$ and E_3 exists if $0 < C < D$ in model (4). Thus, Bogdanov-Takens bifurcation of positive equilibrium is impossible, otherwise it requires $\det(J(E_3)) = 0$ which only occurs at the boundary equilibria E_1 and E_2 . Consequently, $\text{tr}(J(E_3))$ determines the stability of E_3 .

Note that the parameter B does not play any role in determining the stability of E_3 , and it will be shown that it also does not affect the codimension of Hopf bifurcation. It is easy to know that the first term in $\text{tr}(J(E_3))$ is negative for $C < Y_3 < D$. Hence, in order to have Hopf bifurcation, the quadratic polynomial in the second term, $3Y_3^2 - 2(C + D)Y_3 + CD$, must be negative. The roots of the polynomial are

$$Y_{3\pm} = \frac{1}{3}(C + D \pm \sqrt{C^2 + D^2 - CD}). \quad (11)$$

It is easy to show that $Y_{3-} < C < Y_{3+} < D$. This means that E_3 is asymptotically stable for $Y_{3+} \leq Y_3 < D$. A direct computation shows that

$$\text{tr}^*(J(E_3))|_{Y_3=C} = C(D - C) \tanh(C) > 0, \quad (12)$$

$$\text{tr}^*(J(E_3))|_{Y_3=\frac{D}{2}} = \frac{D^2}{4(1 + \cosh(D))} [\sinh(D) - D + 2C] > 0, \quad (13)$$

$$\text{tr}^*(J(E_3))|_{Y_{3+}} = -Y_{3+}(D - Y_{3+})(Y_{3+} - C)(1 - \tanh^2(Y_{3+})) < 0. \quad (14)$$

Thus, $\text{tr}^*(J(E_3)) = 0$ has at least one solution for $Y_3 \in (\max\{C, \frac{D}{2}\}, Y_{3+})$. To prove the uniqueness of the solution, we show $\frac{d\text{tr}^*(J(E_3))}{dY_3} < 0$ for $Y_3 \in (\max\{C, D\}, Y_{3+})$. Note that $C < Y_3 < Y_{3+}$ if $C < D \leq 2C$, and $\frac{D}{2} < Y_3 < Y_{3+}$ if $D > 2C$. A direct calculation shows that

$$C + D - 3Y_3 < \begin{cases} D - 2C \leq 0, & \text{if } \frac{D}{2} \leq C \leq Y_3 < Y_{3+} \text{ for } D \leq 2C; \\ C - \frac{D}{2} < 0, & C < \frac{D}{2} \leq Y_3 < Y_{3+} \text{ for } D > 2C. \end{cases} \quad (15)$$

Further, we have

$$\begin{aligned} \lim_{Y_3 \rightarrow C} \frac{d\text{tr}^*(J(E_3))}{dY_3} &= (C + D - 3Y_3) \cosh^2(Y_3) < 0, \\ \lim_{Y_3 \rightarrow \frac{D}{2}} \frac{d\text{tr}^*(J(E_3))}{dY_3} &= (C - \frac{D}{2})(\cosh(\frac{D}{2}) + \frac{D}{2})(\cosh(\frac{D}{2}) - \frac{D}{2}) < 0, \\ \frac{d^2\text{tr}^*(J(E_3))}{dY_3^2} &= (C + D - 3Y_3)[\sinh(2Y_3) + 2Y_3] - CD \\ &\quad - 3[\cosh(Y_3) + Y_3][\cosh(Y_3) - Y_3] < 0, \text{ for } \max\left\{C, \frac{D}{2}\right\} < Y_3 < Y_{3+}, \end{aligned}$$

which clearly indicates that $\frac{d\text{tr}^*(J(E_3))}{dY_3} < 0$ for $Y_3 \in (\max\{C, \frac{D}{2}\}, Y_{3+})$. That is, $\text{tr}^*(J(E_3))$ is monotonically decreasing for $Y_3 \in (\max\{C, \frac{D}{2}\}, Y_{3+})$. Hence, $\text{tr}^*(J(E_3))$ has a unique solution Y_{3H} for $Y_3 \in (\max\{C, \frac{D}{2}\}, Y_{3+})$, at which Hopf bifurcation occurs. The codimension of Hopf bifurcation can be determined based on the computation of focus values. In order to carry out this analysis, we rewrite $\text{tr}^*(J(E_3))$ as

$$\text{tr}(J(E_3)) = \frac{B}{\sinh(3Y_3)} \text{tr}^*(J(E_3)),$$

where $\text{tr}^*(J(E_3)) = D[Y_3 \sinh(2Y_3) + (Y_3 - C)(\sinh(2Y_3) - 2Y_3)] - Y_3[Y_3 \sinh(2Y_3) + (Y_3 - C)(2 \sinh(2Y_3) - 2Y_3)]$.

It is easy to see that

$$Y_3 \sinh(2Y_3) + (Y_3 - C)(2 \sinh(2Y_3) - 2Y_3) > Y_3 \sinh(2Y_3) + (Y_3 - C)(\sinh(2Y_3) - 2Y_3) > 0$$

for $Y_3 > C$. Therefore, we can find the unique solution for the Hopf critical point, defined in terms of the parameter D (i.e., the K in the original system (2)) as

$$D_H \doteq \frac{Y_3 Y_3 \sinh(2Y_3) + (Y_3 - C) 2 \sinh(2Y_3) - 2Y_3}{Y_3 \sinh(2Y_3) + (Y_3 - C)(\sinh(2Y_3) - 2Y_3)} > Y_3. \quad (16)$$

Note that the critical point Y_{3H} and R_0^H can be determined from D_H :

$$D = D_H \Rightarrow Y_{3H} \Rightarrow R_0^H = \frac{\tanh(C)}{\tanh(Y_{3H})}. \quad (17)$$

Next, applying an affine transformation to system (4) and using the Maple code in Yu [35] for computing the normal form of Hopf bifurcation, we obtain the first-order focus value as follows:

$$v_1 = -\frac{\cosh^2(Y_3)}{8Y_3^2(Y_3 - C)^2}v_1^*, \quad (18)$$

where $v_1^* = C_0C^2 + C_1C + C_2 = C_0\left(C + \frac{C_1}{2C_0}\right)^2 - \frac{C_1^2 - 4C_0C_2}{4C_0}$, and

$$\begin{aligned} C_0 &= (3 \tanh^2(Y_3) - 1)(Y_3 \tanh^2(Y_3) + \tanh(Y_3) - Y_3), \\ C_1 &= -3(Y_3 \tanh^2(Y_3) + \tanh(Y_3) - Y_3)(3Y_3 \tanh^2(Y_3) + \tanh(Y_3) - Y_3), \\ C_2 &= 2Y_3[3 \tanh(Y_3)(1 + Y_3 \tanh(Y_3))(Y_3 \tanh^2(Y_3) + \tanh(Y_3) - Y_3) + \\ &\quad 2Y_3[Y_3^2(1 - \tanh^2(Y_3))]]. \end{aligned} \quad (19)$$

It is obvious that $C_1 < 0$ and $C_2 > 0$, and

$$C_0 \begin{cases} > 0, & \text{if } \tanh^2(Y_3) > \frac{1}{3}, \\ = 0, & \text{if } \tanh^2(Y_3) = \frac{1}{3}, \\ < 0, & \text{if } \tanh^2(Y_3) < \frac{1}{3}. \end{cases}$$

Since $Y_3 \geq C$, C reaches its maximal value at $C = Y_3$. One can show that the term $C_0\left(C + \frac{C_1}{2C_0}\right)^2$ in v_1^* reaches its minimum at $C = Y_3$, regardless of $C_0 > 0$ or $C_0 < 0$. Therefore, for $C_0 \neq 0$, we obtain

$$\begin{aligned} v_1^* &= C_0\left(Y_3 + \frac{C_1}{2C_0}\right)^2 - \frac{C_1^2 - 4C_0C_2}{4C_0} \\ &= \frac{Y_3 \tanh(Y_3)}{\cosh^2(Y_3)[2Y_3 \cosh^2(Y_3) + 3(\frac{1}{2} \sinh(2Y_3) - Y_3)]} > 0. \end{aligned} \quad (20)$$

When $C_0 = 0$, it can be shown that

$$\begin{aligned} v_1^* &= C_1C + C_2 > C_1Y_3 + C_2 \\ &= Y_3[3 \tanh^2(Y_3) + Y_3^2(1 - \tanh^2(Y_3))(3 \tanh^2(Y_3) - 1)] \\ &= Y_3 > 0. \end{aligned} \quad (21)$$

This shows that $v_1^* > 0$, then $v_1 < 0$ for feasible parameter values, which implies that the codimension of the Hopf bifurcation is one, and the Hopf bifurcation is supercritical. Thus, stable limit cycles are expected. The transversal condition can be found as

$$v_0 = \frac{B}{2 \sinh(2Y_{3H})} [Y_{3H} \sinh(2Y_{3H}) + (Y_{3H} - C)(\sinh(2Y_{3H}) - 2Y_{3H})] > 0. \quad (22)$$

In summary, for any given parameters $A > 0$ and $C > 0$, we have $\tanh^{-1}(A) > C$ (i.e., $A > \tanh(C)$) and $Y_3 = \tanh^{-1}(A)$. Then D_H is defined by (16). If $D \leq D_H$, then E_3 is asymptotically stable for $C < Y_3 < D$; if $D > D_H$, then E_3 is asymptotically stable for $C < Y_3 < Y_{3H}$ (Y_{3H} is determined from $D = D_H$), and unstable for $Y_{3H} < Y_3 < D$. Hence, bistable phenomenon happens for $C < Y_3 < Y_{3H}$, and the relaxation oscillation must appear for $R_0 < 1$, but near 1. The above results show that there are no complex dynamical behaviours in system (4) since it does not have Bogdanov-Takens (B-T) bifurcation or generalized Hopf bifurcation. Although the dimensionless system (4) had four parameters, only two

of them (A and C) play important roles in the dynamics of the system, in particular on stability and bifurcation.

Based on the above analysis, we obtain the following results:

Theorem 4.1. *System (4) undergoes the Hopf bifurcation at the threshold Y_{3H} in (17) when $\text{tr}^*(J(E_3))$ in (9) holds, and Y_{3H} defines the unique Hopf critical point. Meanwhile, the Hopf bifurcation is supercritical, yielding stable limit cycles when the first focus value $v_1 < 0$ in (18) is satisfied.*

In order to precisely describe the dynamics transition of equilibrium in system (4), the bifurcation diagram is illustrated in Figure 1, where the basic reproduction number R_0 is taken as the primary bifurcation parameter, solid and dotted lines/curves represent stable and unstable equilibrium solutions, respectively. This bifurcation diagram is a projection on the $R_0 - Y$ plane, clearly shows the bifurcation relation between the four equilibrium solutions: E_0 , E_1 , E_2 and E_3 . The equilibrium E_0 is a stable node, E_1 is always unstable (an unstable node for $R_0 > 1$, and a saddle point for $R_0 < 1$), and E_2 is stable for $0 < R_0 < \frac{\tanh(C)}{\tanh(D)}$. There are two transcritical bifurcations: one of them is at $R_0 = 1$ between E_1 and E_2 , and the other at $R_0 = \frac{\tanh(C)}{\tanh(D)}$ between E_2 and E_3 . The dotted curve on part of E_3 denotes non biologically meaningful solution (only mathematically interesting), and H indicates the supercritical Hopf bifurcation point.

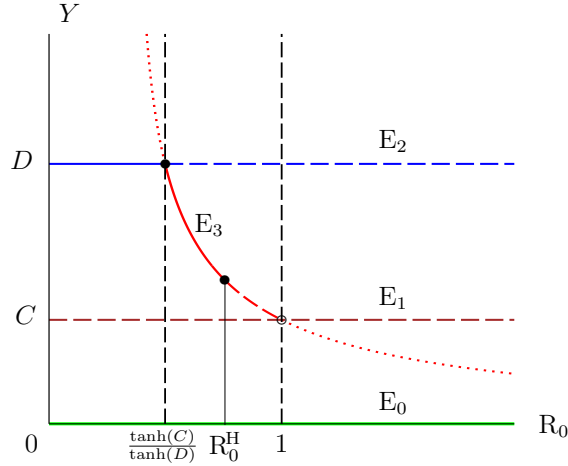


FIGURE 1. Bifurcation diagram for system (4) showing the transition of equilibrium solutions E_0 , E_1 , E_2 , and E_3 , where solid and dotted lines/curves represent stable and unstable equilibrium solutions, respectively.

4.2. Heteroclinic cycle.

Theorem 4.2. *If $0 < C < \tilde{Y} < D$ and $\tanh(C) < A < \tanh(D)$, for an open subset of parameter space, there exists a heteroclinic cycle in the first quadrant connecting equilibria $E_1(0, C)$ and $E_2(0, D)$.*

Proof. We refer to Eduardo's method [12] for the existence of a heteroclinic cycle. The heteroclinic cycle consists of two connections between two saddle points. When $\tanh(C) < A < \tanh(D)$, it is known from section 2 that $E_1(0, C)$ and $E_2(0, D)$

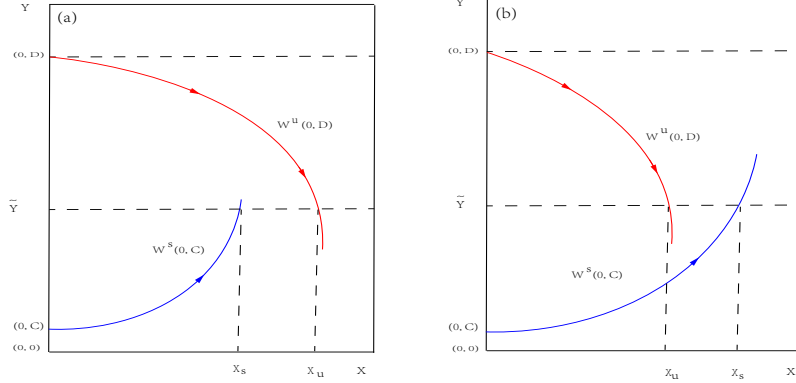


FIGURE 2. The possible relative position between the unstable manifold $W^s(0, C)$ of the saddle point $E_1(0, C)$ and the stable manifold $W^u(0, D)$ of the saddle point $E_2(0, D)$. (a) $X_s < X_u$; (b) $X_s > X_u$.

are both saddle points. Denote the stable and unstable manifolds by $W^s(0, C)$ and $W^u(0, D)$, respectively. The α -limit of $W^s(0, C)$ and the ω -limit of $W^u(0, D)$ are bounded in the X -axis. Neither the ω -limit of $W^u(0, D)$ is on the Y -axis. Let \tilde{Y} satisfy $0 < C < \tilde{Y} < D$. There exist two points $(\tilde{Y}, X_s) \in W^s(0, C)$ and $(\tilde{Y}, X_u) \in W^u(0, D)$, with X_s and X_u depending on the parameter values, such that $X_s = s(A, B, C, D)$ and $X_u = u(A, B, C, D)$ (see Figure 2).

It can be seen from Kuznetsov [17] that one property of heteroclinic connection is that the unstable manifold $W^u(0, D)$ overlaps with the stable manifold $W^s(0, C)$, i.e., $\xi_{DC} \subset W^s(0, C) \cap W^u(0, D)$.

Therefore, there exists $(\tilde{Y}, \tilde{X}) \in \{(Y, X) \in \mathbb{R}^2 | 0 \leq Y \leq D, X \geq 0\}$ such that $\tilde{Y} = \tilde{X}$. Moreover, by the uniqueness of solutions of system (4), this intersection must occur along a whole trajectory ξ_{DC} . Therefore, the equation $s(A, B, C, D) = u(A, B, C, D)$ defines a codimension-one submanifold in the parameter space, for which the heteroclinic curve ξ_{DC} exists in \mathbb{R}_+^2 , connecting the points $E_1(0, C)$ and $E_2(0, D)$. Then $\xi_{DC} \subset W^s(0, C) \cap W^u(0, D)$ and it exists for any parameter value such that $0 < C < Y^* < D$. Hence a heteroclinic cycle ξ exists for certain parameter values on the same submanifold for which $\xi = (0, D) \cup \xi_{DC} \cup (0, C) \cup \xi_{CD}$. \square

5. Numerical simulations. In this section, we will conduct numerical simulations to demonstrate the theoretical results for model (4). We choose the following set of parameters in model (2): $\alpha = 0.99, b = 1.48, r = 1, m = 0.1, K = 1.08, v = 0.01$, which are taken from Fussmann and Blasius [11]. By using the rescalings (3) and (5) for model (4), we have

$$A = 0.1010101, B = 0.4269899, C = 0.0148, D = 1.5984. \quad (23)$$

All figures are drawn by MATLAB and AUTO-07P [8].

Firstly, we verify the existence of heteroclinic cycle based on Theorem 4.2 when $0 < C < \tilde{Y} < D$ and $\tanh(C) < A < \tanh(D)$. Since $C = 0.0148, D = 1.5984$, then we obtain $\tanh(0.0148) < A < \tanh(1.5984)$, i.e., $0.0147989 < A <$

0.9214274. When we take $\alpha = 0.15$ and keep the remaining parameters unchanged in model (2), then we have $A = 0.6666667, B = 2.8181335, C = 0.0148, D = 1.5984$ in model (4), it is easy to obtain that model (4) has two boundary equilibria $E_1(0, 0.0148), E_2(0, 1.5984)$, and one positive equilibrium $E_3(2.1327, 0.80472)$, where E_1 and E_2 are saddles, and E_3 is an unstable focus. There exists a separatrix (the stable manifold of E_1) linked to the boundary equilibrium E_1 , which serves as the boundary of the attraction basins of these two equilibria. Next, we take $\alpha = 0.19$ in model (2), then $A = 0.52631579, B = 2.2248422, C = 0.0148, D = 1.5984$, and model (4) has two boundary equilibria $E_1(0, 0.0148), E_2(0, 1.5984)$, and one positive equilibrium $E_3(1.4291, 0.58504)$, where E_1 and E_2 are saddles, and E_3 is an unstable focus. There exists two heteroclinic orbits: one is connecting two boundary equilibria $E_1(0, 0.0148)$ and $E_2(0, 1.5984)$, and the other is connecting $E_2(0, 1.5984)$ and $E_3(1.4291, 0.58504)$. While $\alpha = 0.99$ in model (2), then $A = 0.1010101, B = 0.42698992, C = 0.0148, D = 1.5984$ in model (4), and there still exist two boundary equilibria $E_1(0, 0.0148), E_2(0, 1.5984)$, both are saddles. The positive equilibrium $E_3(0.055518, 0.10136)$ becomes an unstable focus, see Figure 3 for details.

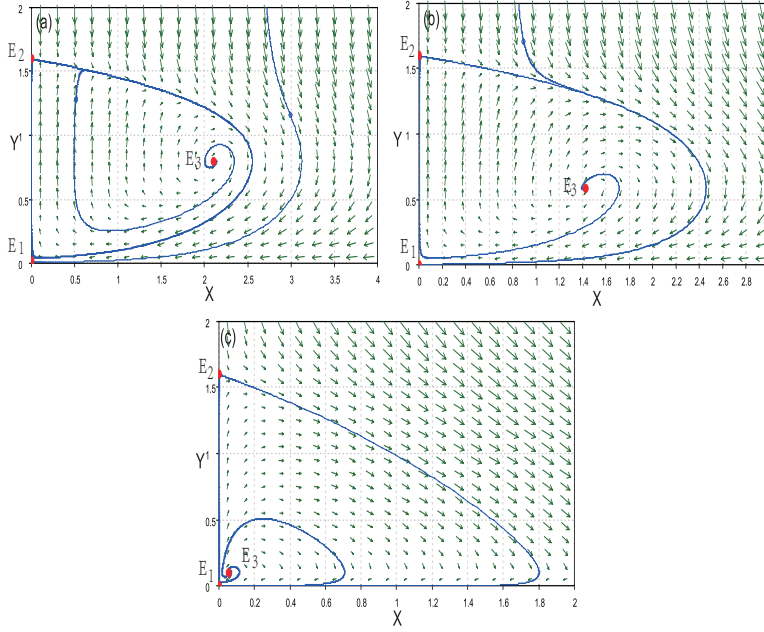


FIGURE 3. Phase portraits of model (4). (a) $A = 0.6666667$ and $B = 2.8181335$. (b) $A = 0.5263158$ and $B = 2.2248422$. (c) $A = 0.1010101$ and $B = 0.4269899$.

To investigate the impact of the basic reproduction number R_0 on the dimensionless system (4), we rewrite it as follows:

$$\begin{aligned} \frac{dX}{d\tau} &= X \left(\tanh(Y) - \frac{\tanh(C)}{R_0} \right), \\ \frac{dY}{d\tau} &= BY(D - Y)(Y - C) - X \tanh(Y). \end{aligned} \tag{24}$$

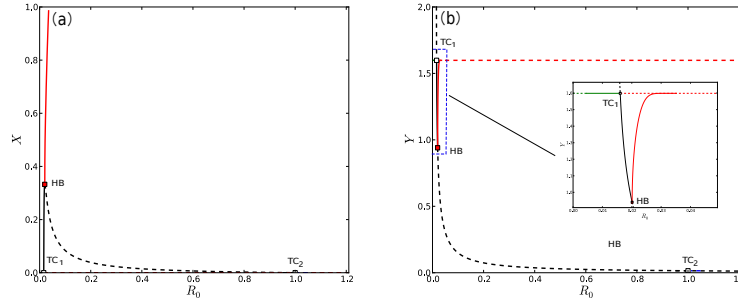


FIGURE 4. Bifurcation diagram for model (24). Here HB , TC_1 and TC_2 denote the supercritical Hopf bifurcation point and two transcritical bifurcation points, respectively. (a) R_0 vs X . (b) R_0 vs Y .

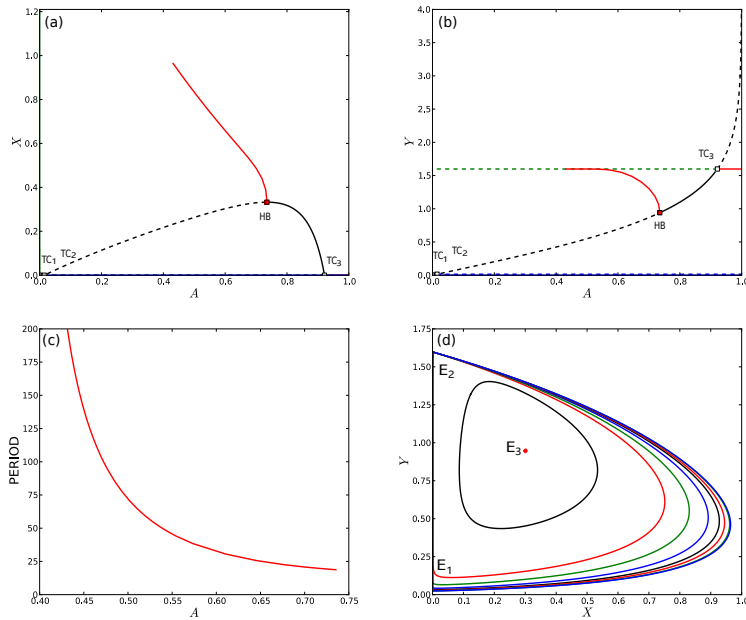


FIGURE 5. Bifurcation diagram and phase portrait of model (4). Here HB , TC_1 , TC_2 and TC_3 denote the supercritical Hopf bifurcation point and three transcritical bifurcation points, respectively. (a) A vs X . (b) A vs Y . (c) A vs the period. (d) A family of stable limit cycles approach a heteroclinic cycle which connects the boundary equilibria $E_1(0, 0.0148)$ and $E_2(0, 1.5984)$.

We take R_0 as the primary bifurcation parameter and choose the parameter values as $B = 0.4269899$, $C = 0.0148$, $D = 1.5984$. Then we obtain one-parameter bifurcation diagram illustrated in Figure 4. There are two transcritical bifurcation points $TC_1(0, 1.59839)$, $TC_2(0, 0.0148)$ and one supercritical Hopf bifurcation point $HB(0.332546, 0.940275)$ as $R_0 = 0.0160609, 1.00, 0.0201250$, respectively. A family

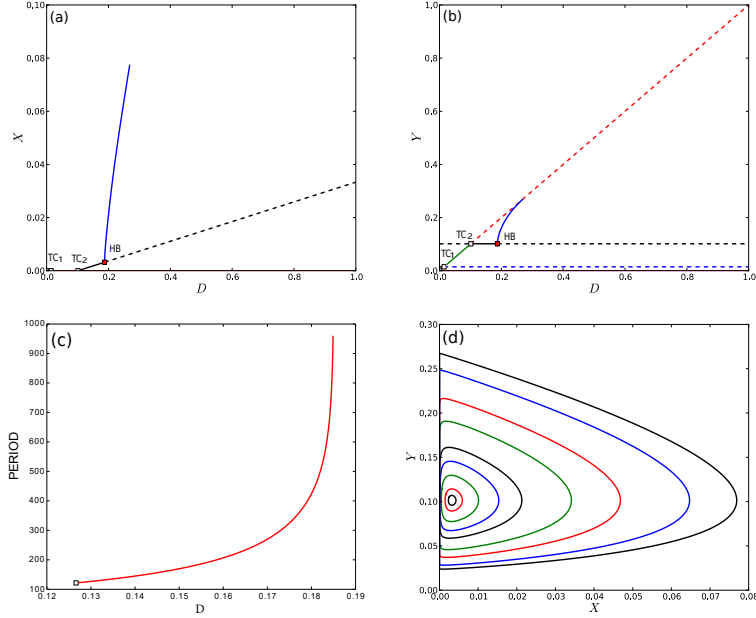


FIGURE 6. Bifurcation diagram and phase portrait of model (4). Here HB , TC_1 and TC_2 denote the supercritical Hopf bifurcation point and two transcritical bifurcation points. (a) D vs X . (b) D vs Y . (c) D vs the period. (d) Heteroclinic relaxation oscillations appear in phase portrait.

of stable limit cycles bifurcating from Hopf bifurcation point HB approach a heteroclinic cycle which connects the boundary equilibria $E_1(0, 0.0148)$ and $E_2(0, 1.5984)$. The bistability regions are, respectively, $(0, \frac{\tanh(C)}{\tanh(D)}) = (0, 0.0160609)$ for the stable equilibrium E_0 and stable equilibrium E_2 ; $(\frac{\tanh(C)}{\tanh(D)}, R_0^H) = (0.0160609, 0.0201250)$ for the stable equilibrium E_0 and the stable equilibrium E_3 ; $(R_0^H, 1) = (0.0201250, 1)$ for the bistable phenomenon involving the stable equilibrium E_0 and a stable limit cycle; $(1, +\infty)$ for the global stability of E_0 .

Secondly, we take the per capita mortality rate of the predator $A (= \frac{m}{\alpha})$ as the primary bifurcation parameter. Choosing $B = 0.4269899$, $C = 0.0148$, $D = 1.5984$ fixed as before, we obtain one-parameter bifurcation diagrams. As shown in Figure 5, there are a supercritical Hopf bifurcation point $HB(0.332546, 0.940277)$ as $A = 0.735349$, and three transcritical bifurcation points $TC_1(0, 0)$ as $A = 0$, $TC_2(0, 0.0148)$ as $A = 0.0147989$, and $TC_3(0, 1.59840)$ as $A = 0.921427$. From Figure 5 (a), it is easy to see that the predator population becomes extinct for all nonnegative initial conditions when the mortality rate A of predators is high enough. By continuation from the supercritical Hopf bifurcation point, we obtain a limit cycle branch and find a family of stable limit cycles approaching a heteroclinic cycle with the period tending to infinity. In other words, the limit cycles are actually approaching a heteroclinic orbit connecting $E_1(0, 0.0148)$ and $E_2(0, 1.5984)$, see Figure 5 (c), (d) for details. That is to say, the predator invasion will cause system (4) to collapse with the increasing per capita mortality of the predator,

namely, the overexploitation occurs as Voorn et al. [31]. Meanwhile, the transition from coexistence to overexploitation is associated with the destruction of periodic solutions. One trivial connection occurs at the boundary of the positive quadrant of the space (X, Y) , from the equilibria E_1 to E_2 , and the other nontrivial connection is from E_2 to E_1 in the interior of the positive quadrant. The region encapsulated by the heteroclinic loop contains the positive equilibrium $E_3(0.332546, 0.940277)$. More interestingly, the so-called hydra effect [7, 26] is also found in model (4), see Figure 5 (a) for details.

Thirdly, we take the carrying capacity $D (= Kb)$ as the primary bifurcation parameter and fix $A = 0.1010101, B = 0.4269899, C = 0.0148$, then we obtain one-parameter bifurcation diagrams. There are one supercritical bifurcation point $HB(3.19134 \times 10^{-3}, 0.101356)$ as $D = 0.187411$, two transcritical bifurcation points $TC_1(0, 0.0148)$ and $TC_2(0, 0.101356)$ as $D = 0.0148$ and $D = 0.101356$, respectively. A family of stable limit cycles bifurcating from the supercritical Hopf bifurcation point HB become heteroclinic relaxation oscillations, see Figure 6. Biologically speaking, the number of predators and the number of prey in system (4) will increase with the increase of carrying capacity. Meanwhile, it is found that heteroclinic relaxation oscillations appear with the increasing periods of limit cycles.

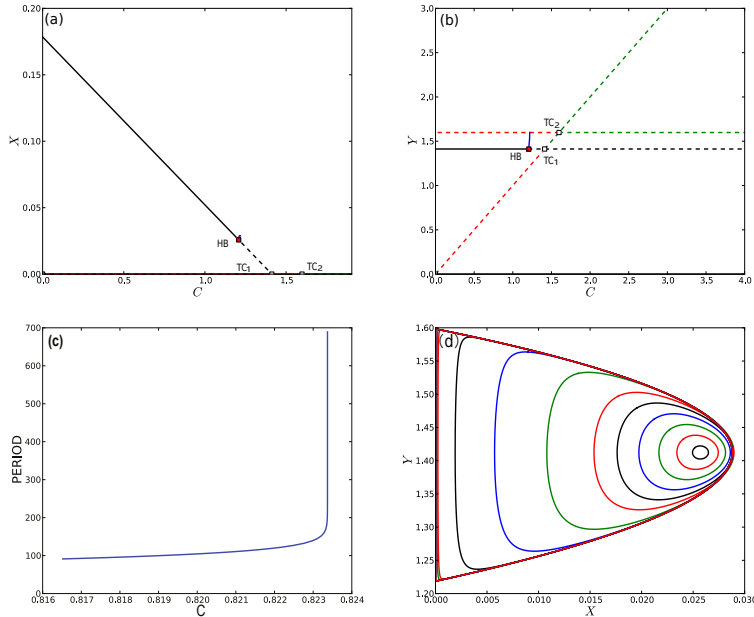


FIGURE 7. Bifurcation diagram and phase portrait of model (4), where HB, TC_1 and TC_2 represent the supercritical Hopf bifurcation point and two transcritical bifurcation points, respectively. (a) C vs X . (b) C vs Y . (c) Period against C . (d) The phase portrait indicates that a family of limit cycles with amplitudes stretched to a heteroclinic cycle connecting $E_1(0, 1.41234)$ and $E_2(0, 1.5984)$.

Now, we investigate the role of strong Allee effect $C (= bv)$ in model (4) with $A = 0.8879899$ (i.e., $m = 0.87911$ in model (2)), and take the Allee effect parameter

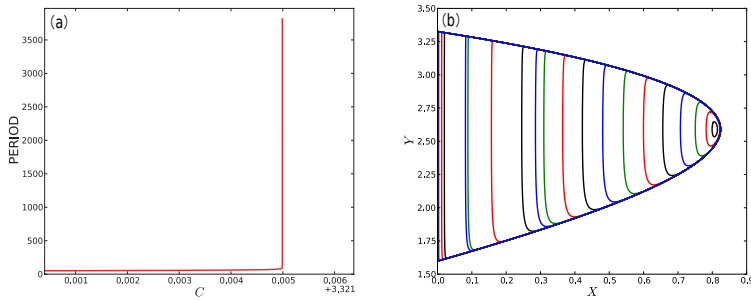


FIGURE 8. (a) Bifurcation diagram (C vs Period) of limit cycles of model (4) as $A = 0.9888$, $B = 0.4269899$, $D = 1.5984$. (b) Heteroclinic relaxation oscillations occur for model (4) with a family of limit cycles approaching a heteroclinic cycle in the phase plane.

C as the free bifurcation parameter. Then we obtain a supercritical Hopf bifurcation point $HB(0.0257627, 1.41234)$ as $C = 1.20845$, and two transcritical bifurcation points $TC_1(0, 1.41234)$ for $C = 1.41234$, $TC_2(0, 1.5984)$ for $C = 1.5984$, see Figure 7 (a), (b). By continuation from the supercritical Hopf bifurcation point, we have a family of stable limit cycles approaching a heteroclinic cycle which connects the equilibria $E_1(0, 1.41234)$ and $E_2(0, 1.5984)$, see Figure 7 (c), (d). Biologically speaking, when the mortality of predators is high, the number of predators will decrease until it becomes extinct as the Allee effect of prey increases.

For comparison, we revisit the dynamics of model (6) without the Allee effect which was investigated by Seo and Wolkowicz [25]. We find that there always exists a saddle-node bifurcation point of limit cycles as the parameter A or D is varied. Further, we notice that the inclusion of the Allee effect may lead to the disappearance of saddle-node bifurcation point of limit cycles. However, it cannot induce the occurrence of isola bifurcation of limit cycles [23, 34].

As we know, global bifurcations have many biological implications. The existence of a heteroclinic cycle has important implications for model (4), which indicates that overexploitation occurs as [15, 31], that is to say, the predator population may eventually go extinct.

At last, we consider the existence of relaxation oscillations as Li et al. [18] in models (6) and (4). Model (6) can exhibit the homoclinic relaxation oscillations which are different from the limit cycles with small amplitudes. This kind of relaxation oscillations occur when the parameter $A \rightarrow 1$. There exists a family of limit cycles approaching the homoclinic cycle which connects the equilibrium E_2 with periods tending to $+\infty$. However, heteroclinic relaxation oscillation cycles rather than homoclinic relaxation oscillation cycles in model (4) can be found, i.e., a family of limit cycles approach a heteroclinic cycle with the period tends to infinity when A is close to 1. Actually, such relaxation oscillations occur when the parameter A in model (4) approaches a constant 0.978912, shown in Figure 8 (a), (b). Interestingly, we find that the heteroclinic relaxation oscillations cycles can be caused by either the strong Allee effect or the high per capita death rate. For the heteroclinic relaxation oscillations cycles caused by the small intrinsic growth rate, it is referred to aforementioned work by Li et al. [18]. More precisely, the existence of heteroclinic cycles is induced by the strong Allee effect, while the relaxation oscillations are caused by the trigonometric functional response.

6. Conclusions. Local bifurcations involved in the dynamics with the equilibria always reflects the transition from one scenario to another, while global bifurcations are associated with the transition from the coexistence of prey and predator to over-exploitation, in particular, the limit cycles are destroyed by homoclinic cycle or heteroclinic cycle. In this paper, we investigate the dynamics in a Rosenzweig–MacArthur predator-prey model with the trigonometric functional response and strong Allee effect. Firstly, we obtain the basic reproduction number and equilibria of model (4). Secondly, we establish sufficient conditions for the local and global asymptotic stability of trivial equilibria in model (4). Thirdly, the local bifurcation and the global bifurcation including transcritical bifurcation, Hopf bifurcation and heteroclinic bifurcation are also given to mark the transition boundaries in parameter interval between different regions and explain the collapse of the Rosenzweig–MacArthur model with the strong Allee effect, respectively. Note that the Bogdanov-Takens bifurcation cannot be found at the positive equilibrium for model (4). Furthermore, we use numerical simulations to verify the theoretical results.

As a comparison to the results in Seo and Wolkowicz [25], the following differences have been observed:

- (1) Model (4) has four equilibria due to the incorporation of the strong Allee effect while model (6) has only three equilibria. The new boundary equilibrium E_1 is attributed to the Allee effect in model (4).
- (2) There is only one supercritical Hopf bifurcation point which can generate large amplitude stable limit cycles in model (4), i.e., the codimension of Hopf bifurcation is one. Model (6) may have two Hopf bifurcation points: one supercritical Hopf bifurcation point and one subcritical Hopf bifurcation point as well as a saddle-node point of limit cycle bifurcation. That is, the involvement of the strong Allee effect may cause the saddle-node bifurcation of limit cycles to disappear. Actually, the saddle-node bifurcation point of limit cycles in model (6) will persist when the parameters A, \bar{B} and D are varied.
- (3) Heteroclinic relaxation oscillations occur for model (4) when A or C is large enough. The heteroclinic cycles in model (4) due to the strong Allee effect while model (6) has only the homoclinic relaxation oscillations. More precisely, the strong Allee effect and the trigonometric functional response may be responsible for the existence of heteroclinic cycle and the occurrence of relaxation oscillations, respectively. Many scenarios have different implications for the dynamics in model (4) due to the occurrence of heteroclinic relaxation oscillations. This scenario does not occur in the models [22, 25].

In this paper, it is noticed that the predation of the predators is more effective when the death rate of the predator is sufficiently small. Biologically speaking, this is true and not surprising. The results show that the Allee effect plays an important role in the stability of model (4) and it is very important to detect the global bifurcations in this model, which helps us understand the dynamics of predators and prey. Interestingly, there exist homoclinic relaxation oscillations similar to those in Zhang et al. [36] or heteroclinic relaxation oscillation for Rosenzweig–MacArthur model which illustrate the recurrence phenomenon or overexploitation, we will leave the analytical proof for future work.

Acknowledgments. The authors are very grateful to the anonymous reviewers and editors for their careful reading and helpful comments, which greatly improve

our manuscript. In addition, the authors are very grateful to Professor Dongmei Xiao for helpful suggestions.

REFERENCES

- [1] C. D. Aline and J. A. Prevedello, [The importance of protected areas for overexploited plants: Evidence from a biodiversity hotspot](#), *Biological Conservation*, **243** (2020), 108482.
- [2] W. Allee, *Animal Aggregations: A Study in General Sociology*, University of Chicago Press, Chicago, USA, 1931.
- [3] L. Berec, V. Bernhauerova and B. Boldin, [Evolution of mate-finding Allee effect in prey](#), *J. Theoret. Biol.*, **441** (2018), 9–18.
- [4] S. Biswas, S. K. Sasmal, S. Samanta, M. Saifuddin, Q. J. A. Khan and J. Chattopadhyay, [A delayed eco-epidemiological system with infected prey and predator subject to the weak Allee effect](#), *Math. Biosci.*, **263** (2015), 198–208.
- [5] C. Castillo-Chavez, et al., *Mathematical Approaches for Emerging and Reemerging Infectious Diseases: An Introduction*, Springer-Verlag, New York, 2002.
- [6] S. N. Chow and J. K. Hale, *Methods of Bifurcation Theory*, Springer, New York, 1982.
- [7] M. H. Cortez and P. A. Abrams, [Hydra effects in stable communities and their implications for system dynamics](#), *Ecology*, **97** (2016), 1135–1145.
- [8] E. J. Doedel and B. E. Oldeman *AUTO-07P: Continuation and Bifurcation Software for Ordinary Differential Equations*, Technical report, Concordia University, 2009.
- [9] K. J. Duffy, K. L. Patrick and S. D. Johnson, [Does the likelihood of an Allee effect on plant fecundity depend on the type of pollinator?](#), *Journal of Ecology*, **101** (2013), 953–962.
- [10] N. T. Fadaei and M. J. Simpson, [Population dynamics with threshold effects give rise to a diverse family of Allee effects](#), *Bull. Math. Biol.*, **82** (2020), 74, 22 pp.
- [11] G. F. Fussmann and B. Blasius, [Community response to enrichment is highly sensitive to model structure](#), *Biology Letters*, **1** (1992), 9–12.
- [12] E. González-Olivares, B. González-Yañez, J. Mena Lorca, A. Rojas-Palma and J. D. Flores, [Consequences of double Allee effect on the number of limit cycles in a predator-prey model](#), *Comput. Math. Appl.*, **62** (2011), 3449–3463.
- [13] D. W. Goodsman, D. Koch, C. Whitehouse, M. L. Evenden, B. J. Cooke and M. A. Lewis, [Aggregation and a strong Allee effect in a cooperative outbreak insect](#), *Ecological Applications*, **26** (2016), 2623–2636.
- [14] W. M. Hirsch, H. Hanisch and J. P. Gabriel, [Differential equation models of some parasitic infections: Methods for the study of asymptotic behavior](#), *Comm. Pure Appl. Math.*, **38** (1995), 733–753.
- [15] P. Ilaria, B. Ugo, E. A. Toufic and L. Alessandro, [Dynamic patterns of overexploitation in fisheries](#), *Ecological Modelling*, **359** (2017), 285–292.
- [16] A. D. Jassby and T. Platt, [Mathematical formulation of the relationship between photosynthesis and light for phytoplankton](#), *Limnology and Oceanography*, **21** (1976), 540–547.
- [17] Y. A. Kuznetsov, *Elements of Applied Bifurcation Theory*, Applied Mathematical Sciences, Springer-Verlag, New York, 1998.
- [18] M. Y. Li, W. Liu, C. Shan and Y. Yi, [Turning points and relaxation oscillation cycles in simple epidemic models](#), *SIAM J. Appl. Math.*, **76** (2016), 663–687.
- [19] J. L. Orrock, R. D. Holt, M. L. Baskett, [Refuge-mediated apparent competition in plant-consumer interactions](#), *Ecology Letters*, **13** (2010), 11–20.
- [20] S. V. Petrovskii, A. Y. Morozov and E. Venturino, [Allee effect makes possible patchy invasion in a predator-prey system](#), *Ecology Letters*, **5** (2002), 345–352.
- [21] L. A. D. Rodrigues, D. C. Mistro and S. Petrovskii, [Pattern formation in a space- and time-discrete predator-prey system with a strong Allee effect](#), *Theoretical Ecology*, **5** (2012), 341–362.
- [22] M. L. Rosenzweig and R. H. MacArthur, [Graphical representation and stability conditions of predator-prey interactions](#), *The American Naturalist*, **97** (1963), 209–223.
- [23] B. Sandstede and Y. Xu, [Snakes and isolas in non-reversible conservative systems](#), *Dyn. Syst.*, **27** (2012), 317–329.
- [24] S. K. Sasmal and J. Chattopadhyay, [An eco-epidemiological system with infected prey and predator subject to the weak Allee effect](#), *Math. Biosci.*, **246** (2013), 260–271.

- [25] G. Seo and G. S. K. Wolkowicz, [Sensitivity of the dynamics of the general Rosenzweig–MacArthur model to the mathematical form of the functional response: A bifurcation theory approach](#), *J. Math. Biol.*, **76** (2018), 1873–1906.
- [26] D. K. Sorenson and M. H. Cortez, [How intra-stage and inter-stage competition affect overcompensation in density and hydra effects in single-species, stage-structured models](#), *Theoretical Ecology*, **14** (2020), 23–39.
- [27] D. Start and B. Gilbert, [Plant sex alters Allee effects in aggregating plant parasites](#), *Oikos*, **127** (2018), 792–802.
- [28] P. A. Stephens, W. J. Sutherland, R. P. Freckleton, [What is the Allee effect?](#), *Oikos*, **87** (1999), 185–190.
- [29] J. Sugie and Y. Saito, [Uniqueness of limit cycles in a Rosenzweig–MacArthur model with prey immigration](#), *SIAM J. Appl. Math.*, **72** (2012), 299–316.
- [30] P. van den Driessche and J. Watmough, [Reproduction numbers and sub-threshold endemic equilibria for compartmental models of disease transmission](#), *Math. Biosci.*, **180** (2002), 29–48.
- [31] G. A. K. van Voorn, L. Hemerik, M. P. Boer and B. W. Kooi, [Heteroclinic orbits indicate over-exploitation in predator-prey systems with a strong Allee effect](#), *Math. Biosci.*, **209** (2007), 451–469.
- [32] M. Verma, [Modeling the effect of rarity value on the exploitation of a wildlife species subjected to the Allee effect](#), *Nat. Resour. Model.*, **29** (2016), 470–494.
- [33] J. Wang, J. Shi and J. Wei, [Predator-prey system with strong Allee effect in prey](#), *J. Math. Biol.*, **62** (2011), 291–331.
- [34] Y. Xu, Z. Zhu, Y. Yang and F. Meng, [Vectored immunoprophylaxis and cell-to-cell transmission in HIV dynamics](#), *Internat. J. Bifur. Chaos Appl. Sci. Engrg.*, **30** (2020), 2050185, 19 pp.
- [35] P. Yu, [Computation of normal forms via a perturbation technique](#), *J. Sound Vibration*, **211** (1998), 19–38.
- [36] W. J. Zhang, M. W. Lindi and P. Yu, [Viral blips may not need a trigger: How transient viremia can arise in deterministic in-host models](#), *SIAM Review*, **56** (2014), 127–155.

Received December 2020; 1st revision July 2021; final revision February 2022; early access May 2022.

E-mail address: victorlxq@163.com

E-mail address: Yancong@hznz.edu.cn

E-mail address: dzgao@shnu.edu.cn

E-mail address: fan_guihong@columbusstate.edu